A New Method for the Discovery of the Distant Exoplanets

Lerner, Peter; Mayer, Alexandre; Sullivan, Thomas E

Published in:
Proceedings of SPIE

DOI:
10.1117/12.2687314

Publication date:
2023

Document Version
Early version, also known as pre-print

A New Method for the Discovery of the Distant Exoplanets

P. B. Lerner[1], A. Mayer[2], T. E. Sullivan[3]

Abstract

Since the first confirmed discovery of exoplanets in 1992, multiple observational methods have been developed. Most methods of their discovery use the influence of a planet on its host star. These methods lose sensitivity when a planet is distant from its star and has a long orbital period. This article proposes a method inspired by Hanbury-Brown Twiss (HBT) interferometry, to find exoplanets which exercise a very small influence on their host star. Our method relies on an extremely high sensitivity of the phase correlations to an asymmetry of the luminous system.

1. Introduction

The extant methods of exoplanet discovery are largely based on the non-stationarity of the back-action of the exoplanet on the host star or other exoplanets (Fischer D. A. 2014), (Bozza 2016). They are poorly suitable for the exoplanets that are distant from the host star because their back-action on the host star changes too slowly during a typical time of astronomical observation. In this paper, we suggest using intensity interferometry, which amplifies the asymmetry of the correlation function of the observed compound object (star + planet). Because of the discontinuity of the phase variation of the correlation function, this method has no fundamental bounds, being restricted only by instrumental limitations.

Current methods of the discovery of exoplanets other than direct imaging are four-fold. First, it is an observation of the darkening of the disk of the host star during transit. Second, it is Doppler spectroscopy, which registers the modulation of the spectral lines because of the center-of-mass motion of the star system. Doppler spectroscopy was historically the first method, and, naturally, the first observations were large planets close to their star, i.e., “Hot Jupiters," hardly conducive to habitability. Third, it is the transit-timing method, which analyses anomalies in the motion of other

[1] Self.
[2] Physics Department, University of Namur, Belgium.
[3] Temple University, professor emeritus, died 05/30/2023.

exoplanets in the system. Fourth, it is microlensing – the imaging of the planetary system using gravitational lensing of the star.

All these methods, except microlensing, involve the planet's back-action on the host star's system. However, these methods would be difficult to implement even for the planets of the Solar System. For instance, Neptune traverses the solar diameter for three days out of 60,195 days of its orbital period. If these are missed, one must wait 165 years for the repetition. Microlensing works best when the planet is close to the apogee of its host star as seen from the Earth and presumes half of the orbital period—more than 30,000 days wait if the observation was missed. The barycentric velocity of the Sun-Neptune system is a meager 1 km/hr ($v = \frac{2\pi\, a_B}{T_{Neptune}}$). Neptune's orbital motion produces a Doppler shift of the solar spectral lines on the order of 10^{-9}. This shift is easily masked by the interference of larger planets such as Jupiter and the Doppler and collisional broadening.

The transit-timing method presumes the existence of other, already discovered bodies in the planetary system. Their orbit parameters must be well known and compared with the Kepler law within the necessary degree of precision. This paper proposes an alternative based on the superresolution available with the phase contrast methods. That is, amplitude image resolution obeys the Rayleigh criterion. On the contrary, phase diagnostics is limited only by instrumental considerations (Shouten 2003)[4](Cotte 2011).

On Earth, we obtain only the amplitude distribution of astronomical objects because of the gigantic phase obtained by the starlight on its propagation. However, intensity interferometry with a photon count eliminates a common phase shift of the photons propagating from a star or reflected from a planet.

Diverse applications of the Brown-Twiss interferometry were reviewed by (Baum 1997). His review paper emphasized that the Brown-Twiss detection rate is expressed through a Fourier transform of the density distribution.

For example, we consider a uniformly lit system with the x-axis along the line connecting the centers of a star and a planet and the observation in the direction of the star's center. The amplitude of the signal from an entire system is not sufficiently different from that of an isolated star. A

[4] Shouten et *op. cit.* described the phase singularities with infinite derivatives but did not present a measurement procedure leading to superresolution. Currently, the superresolution of phase images is widely used in biological imagery.

completely different picture is observed when we register the quadratures of the signal. In the chosen geometry, the cosine quadrature reproduces the signal from the star alone. In contrast, the sine quadrature emphasizes the difference between the Fourier image of the star and the planet.

2. An outline of the method

Diverse applications of the Brown-Twiss interferometry were reviewed by (Baum 1997). In his review paper, he demonstrated that the Brown-Twiss detection could be expressed through a Fourier transform of the density distribution:

$$C(\vec{q}) - 1 = \left| \int \rho(\vec{r}) e^{i\vec{q}\cdot\vec{r}} \, d^3r \right|^2 \quad (1)$$

In Equation (1), $\rho(\mathbf{r})$ is a three-dimensional density distribution of the luminous object, $\mathbf{q}=\mathbf{k}_1-\mathbf{k}_2$ is a spatial frequency, $\mathbf{k}_i=k\cdot\mathbf{r}_i$, are the wavevectors in the direction of the detector i=1,2, and C(**q**) is an intensity correlation coefficient:

$$C(\vec{q}) = \frac{<I_1 I_2>}{<I_1><I_2>}. \quad (2)$$

Naturally, in the case of astronomical observation, the density distribution is effectively two-dimensional because we observe a projection of an object on a focal plane of the registering device.

As an example, we consider a uniformly lit object of the following configuration presented in Fig. 1:

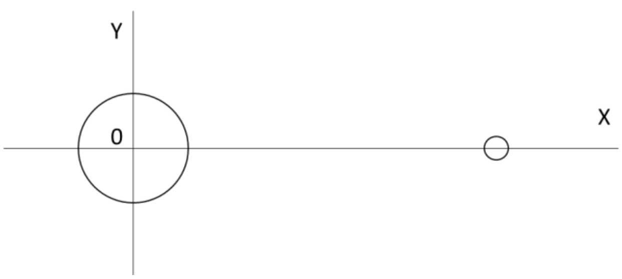

Fig. 1 The geometry of the image (not in scale). Observation is directed at the center of the star. The planet is located along the X-axis.

For the clarity of our demonstration, we present a system star+planet with the following characteristics. The planet has a 1/10 radius of the host star, a distance of 10 diameters from the host star, and a luminosity of 10^{-4} of the star, which presumes an albedo close to unity and negligible thermal radiation of the planet. The amplitude of the signal from an entire system is not sufficiently different from the star's signal alone. A completely different picture is observed when we register the quadratures of the signal defined according to the formulas:

$$C_{system} = \left|F_{star}(q) + F_{planet}(q)\right|^2 Cos\left[2\,Arg\left(F_{star}(q) + F_{planet}(q)\right)\right]$$
$$S_{system} = \left|F_{star}(q) + F_{planet}(q)\right|^2 Sin\left[2\,Arg\left(F_{star}(q) + F_{planet}(q)\right)\right] \quad (3)$$

where F(.) is a Fourier transform of the luminous density profile. In the chosen geometry of Fig. 1, the cosine quadrature reproduces the signal from the star alone (Fig. 2). The sine quadrature emphasizes the difference between the Fourier image of the star and the planet. A-priori amplitude of the sine quadrature is proportional to $\sqrt{I_{star} I_{planet}}$, i.e., a few percent of the amplitude of a star alone. The image in Fig. 3 confirms this intuition.

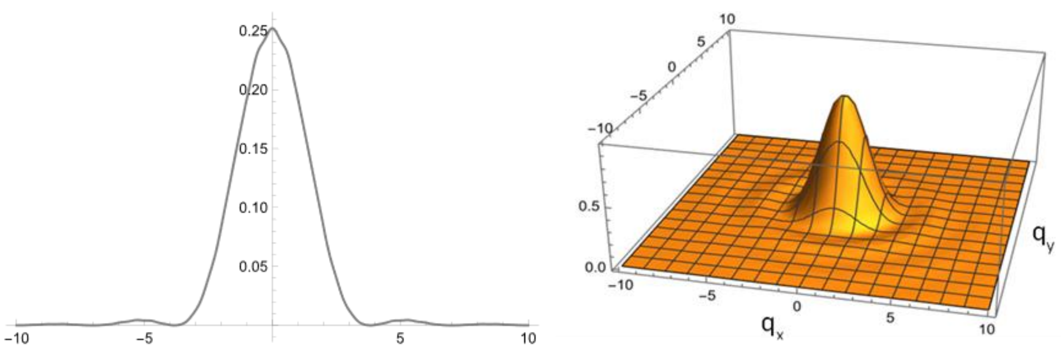

A) B)

Fig. 2 A) Brown-Twiss profile of the system in geometry of Fig. 1. B) Cosine quadrature of the Brown-Twiss signal (Equation 4). q_x and q_y are the spatial frequencies.

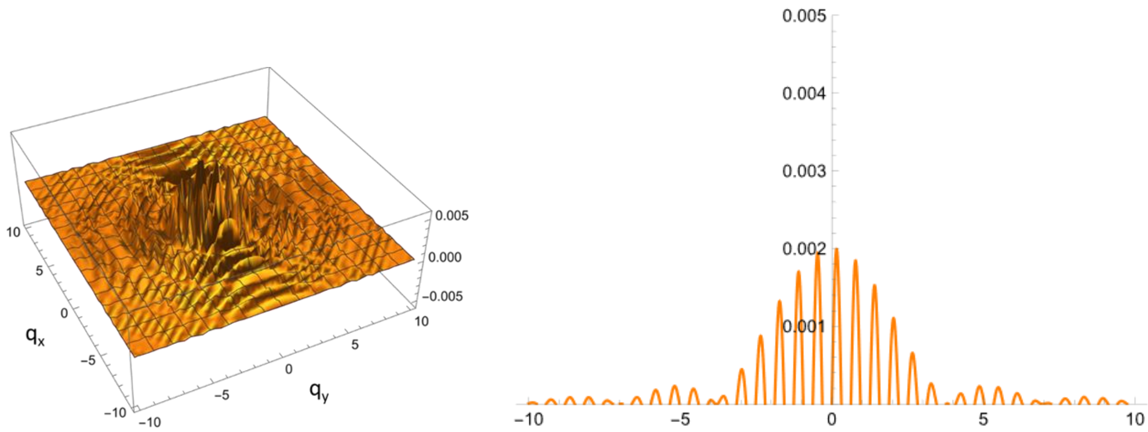

Fig. 3 A) Sine quadrature of the Brown-Twiss signal (see Equation 4), B) Cross-section of the sine quadrature of the signal.

In that case, a Fourier transform of a planet's image can be expressed as a shifted Fourier transform of the centered planet's image. Fig. 3 shows that the sine quadrature displays sharp peaks with discontinuous derivatives.

$$
\begin{aligned}
C_{system} &= \left|F_{star}(q) + e^{iqa}\tilde{F}_{planet}(q)\right|^2 Cos\left[2\,Arg\left(F_{star}(q) + e^{iqa}\tilde{F}_{planet}(q)\right)\right] \\
S_{system} &= \left|F_{star}(q) + e^{iqa}\tilde{F}_{planet}(q)\right|^2 Sin\left[2\,Arg(F_{star}(q) + e^{iqa}\tilde{F}_{planet}(q))\right]
\end{aligned} \tag{4}
$$

In Equation (4) variable with a tilde is a Fourier transform of a planet's distribution at the origin, and a is the difference in optical paths in channels 1 and 2 (see the next section). We shall discuss a practical way to determine quadratures in the next section.

3. **Detection of quadratures of the signal**

Two types of intensity measurements are possible in the arms of the Brown-Twiss interferometer. First, it is the average intensity of light passing through an interferometer:

$$
< I(\vec{r},t) >=< I_1(\vec{r},t) > +< I_2(\vec{r},t) > +2[< I_1(\vec{r},t) >< I_2(\vec{r},t) >]Re(\gamma(\vec{r}_1,\vec{r}_2)) \tag{5}
$$

The Equation (5) is derived, for instance, in (Mandel, 1995), Chapter 4.3. In Equation (5), $\gamma(\vec{r}_1,\vec{r}_2)$ is the normed intensity correlation function:

$$
\gamma(\vec{r}_1,\vec{r}_2) = \frac{Tr<\vec{E}_1(\vec{r}_1)\otimes\vec{E}(\vec{r}_2)>}{<I_1(\vec{r}_1)>^{1/2}<I_2(\vec{r}_2)>^{1/2}} \tag{6}
$$

In Equation (5), we assume that the arms of an interferometer are symmetric. Another observable quantity is the Michelson visibility of the interference pattern defined as:

$$M(\vec{r}) = \frac{I_{max}(\vec{r}) - I_{min}(\vec{r})}{I_{max}(\vec{r}) + I_{min}(\vec{r})} = 2\left(\sqrt{\frac{<I_1(\vec{r},t)>}{<I_2(\vec{r},t)>}} + \sqrt{\frac{<I_2(\vec{r},t)>}{<I_1(\vec{r},t)>}}\right)^{-1} |\gamma(\vec{r}_1,\vec{r}_2)| \quad (7)$$

Michelson visibility is proportional to $|\gamma(\vec{r}_1,\vec{r}_2)|$ (Mandel and Wolf, Equation (4.3-25)). Combining the Equations (5) and (7), we obtain a formula for the argument of the correlation function:

$$Arg(\gamma) = Arccos\left[\frac{2<I(\vec{r},t)>}{<I_1(\vec{r},t)> + <I_2(\vec{r},t)>} - 1\right] \quad (8)$$

From Equation (8), it is evident that the argument of the Arccosine lies in an interval [-1, 1]. Certainly, the imaginary part and, hence, the argument of the correlation function can be obtained from the Hilbert transform of the $Re(\gamma(\vec{r}_1,\vec{r}_2))$ only, but this requires knowledge of the correlation function across all dynamical ranges, which is hard to achieve in practice.

4. A sketch of the experimental setup

The measurement of the quadratures can be accomplished through a binocular setting of two telescopes. A required dynamical range of the telescopes in the pair is assumed to be between the correlation radius $r_c \sim \lambda/\Delta\theta_{s+p}$ of the entire planetary system and the correlation radius $r_c \sim \lambda/\Delta\theta_s$ of the luminous star. Here λ is the observation wavelength, $\Delta\theta_s$ is the angular dimension of the star, and $\Delta\theta_{s+p}$ – is the angular dimension of the prospective system. For an imaginary system of the size of five a.u. at the distance of 10 parsec illuminated by the dwarf star with 15% of the diameter of the Sun observed at 0.5 micron, a requisite dynamical range will be between 2 meters and 10 kilometers. Alternatively, using a 100 GHz submillimeter array, a dynamical range increases to 1.3 km and 6,600 km. These distances between detectors are accessible through Very Large Baseline Interferometry (VLBI, (Bowman 2016), (Vincent 2016)). From the above crude estimates, it seems that a mid-infrared range of observation might be optimal.

We provide a possible sketch of the setup in Fig. 4.

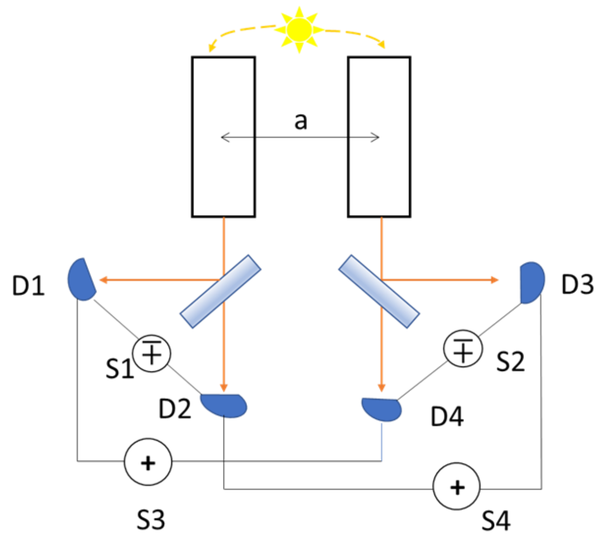

Fig. 4 A possible experimental setup for the measurement of the Brown-Twiss quadratures. The distance *a* is the dynamic range of an interferometer. $D_{1,2,3,4}$ are the photon detectors, and $S_{1,2,3,4}$ are the coincidence (anti-coincidence) counters. Counters $S_{1,2}$ measure $< I >$, $< I_2 >$ and $< {I_1}^2 >$, $< {I_2}^2 >$. Counters $S_{3,4}$ measure $< I_1 \cdot I_2 >$. Varying *a* – the distance between telescopes, one can infer the sine and cosine quadratures (Equations (5) and (8)) from these data.

Once photon counts in the interferometer's two arms are balanced and their stationarity established, one can independently measure the intensity fluctuations in each arm and the coincidence count between the arms. According to the results of the previous section and Equations (4.3-5 and 4.3- (23-25)) of Mandel and Wolf, these measurements can establish the quadratures of Equations (3) and (4) (Mandel 1995). Orthogonal quadratures can confirm or deny the existence of an exoplanet — practically, whether the luminous object is circularly symmetric or not. The advantage of the method is that it seems extremely sensitive to the asymmetry of the target despite a great disparity in luminosities.

5. **Conclusion**

Our paper proposes a method of exoplanet discovery inspired by the Hanbury-Brown-Twiss interferometry. This method is particularly suitable for discovering the exoplanets, which are distant from the host star and influence it only slightly. This method relies only on the asymmetry of the spectral image. An increase in resolution with respect to the Rayleigh criterion is possible because the fluctuations in the photo-current depend on the correlation between distant detectors. While the correlation between distant detectors is perfectly classical ((Mandel 1995), Ch. 4), the gain in resolution can be obtained only through the photon counting methods.

References

Baum, G. 1997. "The Physics of Hanbury Brown-Twiss Interferometry: from Stars to Nuclear Collisions." *XXXVI Cracow School of Theoretical Physics.* Zakopane.

Bowman, K. L., M. D. Johnson, and D. Zoran. 2016. "Computational imaging for VLBI image reconstruction." In *2016 IEEE Conference on Computer Vision and Pattern Recognition*.

Bozza, V., Mancini, L. and A. Sozetti (eds.). 2016. *Methods of detecting exoplanets.* Heidelberg: 2016.

Cotte, Y., M. F. Toy, C. Depeursinge. 2011. "Beyond the lateral resolution in phase imaging." *Journal of Biomedical Optics* 16 (10): 106007.

Fischer D. A., A. W. Howard, G. P. Laughlin, B. Macintosh, S. Mahadevan, J. Salmann, and J. C. Yee. 2014. "Exoplanet Detection Techniques." In *Protostars and Planets VI*, by Beuther H. et al., 715-737.

Mandel, L. and E. Wolf. 1995. *Optical Coherence and Quantum Optics.* Cambridge University Press.

Shouten, H. F., G. Gbur, T. D. Visser and E. Wolf. 2003. "Phase singularities of the coherence functions in Young's interference pattern." *Optics Letters* 28 (12): 968-970.

Vincent, L., S. Doelman, W. T. Freeman. 2016. "Computational imaging for VLBI image reconstruction." In *2016 IEEE Conference on Computer Vision and Pattern Recognition*.